SIMULATIONS ON REDUCING THE INFLUENCE OF BACKSCATTERED SLOW POSITRONS ON LIFETIME MEASUREMENTS

Doru DINESCU [1, 2], Nikolay DJOURELOV [3]

In e^+ lifetime measurements with slow e^+, incident e^+ hit the target and a fraction of them is backscattered. If the backscattered e^+ reach back the accelerator they can be reflected by the electric field and implanted into the sample with a delay, causing spectrum distortions. The method of guiding the e^+ through a bent tube equipped with steering coils will be implemented at the ELI-NP e^+ line. To understand the origin of these distortions and to further improve the performance of the system, comprehensive Comsol Multiphysics and Geant4 simulations were performed.

Keywords: slow positron, backscattering, positron lifetime, Comsol, Geant4

1. Introduction

For the development of new functional materials, the investigation of lattice defects and various atomic imperfections in solids constitutes an important step. Conventional positron annihilation methods use energetic e^+ directly emitted from radioisotopes such as ^{22}Na and are suited to study bulk materials. For analyzing subsurface layers and thin films, slow e^+ beams are necessary [1]. At the European Light Infrastructure – Nuclear Physics (ELI-NP), a brilliant γ-beam will produce fast e^+ by the pair production mechanism in a suitable converter made of tungsten foils, which also act as the e^+ moderator [2].

One of the positron annihilation techniques, which over the years has become an increasingly valuable tool for study of the defect structure in materials, is the Positron Annihilation Lifetime Spectroscopy (PALS) [3]. PALS is based on measuring the lifetime of a e^+ within a solid. Conventional PALS, which most often uses a ^{22}Na source, is a precise timer which measures the time between the 1274 γ-quantum released at the beta plus decay and one of the two 511 γ-quanta emitted through the annihilation of the positron with an electron from the studied material.

[1] PhD student, University POLITECHNICA of Bucharest, PhD School in Engineering and Applications of Lasers and Accelerators, e-mail: doru.dinescu@eli-np.ro
[2] PhD Research Assistant, Extreme Light Infrastructure - Nuclear Physics, Horia Hulubei National Institute for Physics and Nuclear Engineering,
[3] Senior Researcher II, Extreme Light Infrastructure - Nuclear Physics, Horia Hulubei National Institute for Physics and Nuclear Engineering, e-mail: nikolay.djourelov@eli-np.ro

In order to perform PALS with a slow e^+ beam a start signal is needed. Different methods have been designed and successfully applied for the generation of a start signal: detection of secondary e^- produced by incident e^+ [4], e^+ accumulated in a Penning trap and released by a trigger [5], and chopping and bunching technique to form ultra-short e^+ pulses [6].

For depth profiling purposes, the slow e^+ are accelerated by a few graded electrodes to a desirable energy up to typically 30 keV. When incident e^+ hit the target a fraction of them is backscattered. If the backscattered e^+ reach back the accelerator they can be reflected by the electric field and implanted into the sample with a delay from the initial e^+ bunch. This causes significant distortions in the PALS spectrum as satellite peaks [7-9]. In order to suppress the satellite structures several methods have been applied: passing the accelerated incident e^+ through a E×B filter [10], implementing an accelerator-decelerator structure [11], or guiding the e^+ through a 45° bent tube equipped with steering coils after they pass through the accelerator [7]. The last method is foreseen to be implemented in the designed pulsing system for the ELI-NP positron beam.

The aim of the study conducted in the present paper is to determine the optimum parameters of the designed system in order to obtain PALS spectra with minimum distortions caused by the backscattered e^+.

2. Setup, simulation and analysis

Comsol Multiphysics was used for simulating the magnetic field that will guide the e^+ beam from the accelerator to the center of the sample, and for the generation of the electric field of the accelerator [12]. The magnetic field was generated by a series of multi-turn Helmholtz coils. Fig. 1 presents the surface plot of the magnetic and the contour lines of the electric 3D maps on a cross section along the central axis. The magnetic field is close to uniform (60 ± 2 G) along the axis. The electric field used for the acceleration of the particles towards the sample was obtained by applying a potential U_{acc} equally spread on the graded electrodes (having holes with diameter D = 60 mm) of the accelerator. The Faraday cage with internal diameter 116 mm and length of 720 mm was kept at the potential U_{acc} to act as a e^+ drift region.

The 3D maps of the Comsol simulations were exported into an ASCII format in which the values of the magnetic and electric fields were taken point by point in a grid pattern, and imported into the Geant4 software where the simulations regarding e^+ backscattering were performed. The Geant4 simulations were performed using the low energy physics model G4EmLivermorePhysics which includes ionization, bremsstrahlung and multiple scattering. The geometry built in Comsol was reproduced in Geant4, thus the magnetic and electric fields, which were imported, perfectly overlap with the beam transport lines. This was

crosschecked by monitoring whether the primary e^+ beam trajectories, simulated using the Geant4 software, hit the target center.

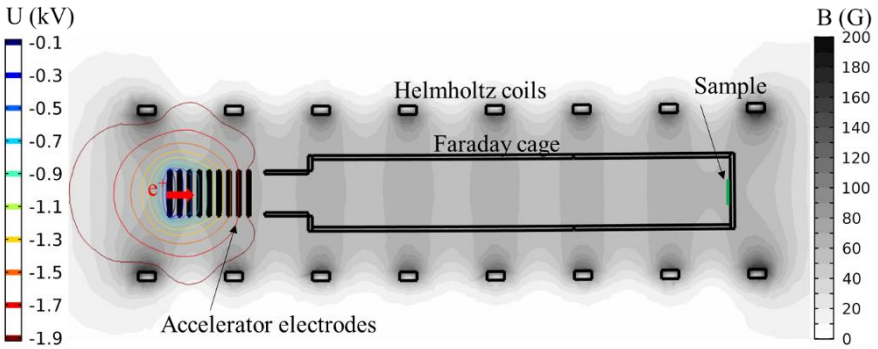

Fig. 1. The cross section of the 3D maps along the central beam line axis represented by a surface plot of the magnetic field and contour lines of the electric field in the case of a straight tube and potential U_{acc}= -2 kV.

For each Geant4 simulation 1×10^6 e^+ were shot towards the sample. The e^+ backscattering coefficient is strongly dependent on the average atomic number *Z*. The higher *Z*, the more the backscattering [13]. Our choice of a sample with relatively low *Z*, namely silicon with $Z = 14$, aims to underline the significance of the studied effect. Fig. 2 shows an example of e^+ trajectories as obtained by Geant4 for low statistics. It is seen that the accelerated e^+ hit the sample, a fraction of them are backscattered, then reach the accelerator, where they are reflected, and are finally reimplanted into the sample.

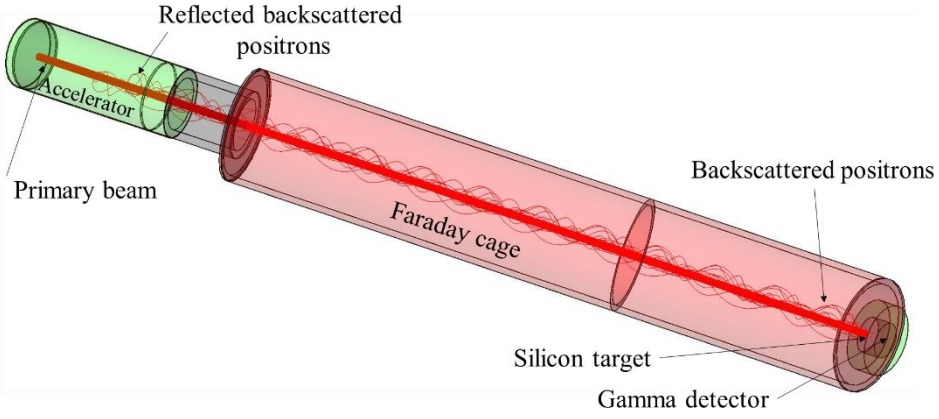

Fig. 2. The trajectories of the primary 2 keV e^+ beam and the event of e^+ backscattering with 300 incident particles. Example of a straight tube obtained by Geant4.

Fig. 3a presents the time of annihilation within the target for e^+ accelerated to E_+= 2 keV in a straight geometry as shown in Fig. 2. The very sharp peak corresponds to e^+ which are directly implanted into the target. The very broad peak is due to backscattered e^+ reflected from the accelerator electric field and then implanted into the target. The delayed e^+ can significantly distort the long-lived components when measuring a PALS spectrum.

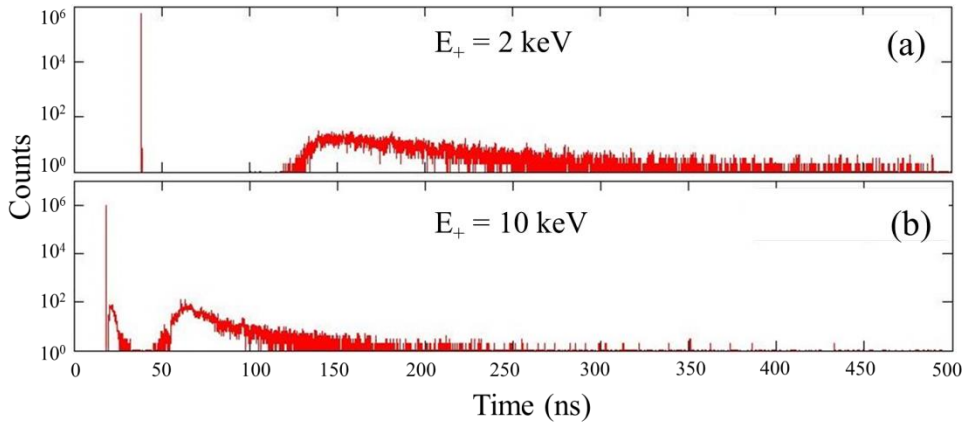

Fig. 3 Histogram of the time at which the e^+ annihilate within the target for the geometry shown in Fig. 2. Case a) e^+ accelerated to E_+= 2 keV and case b) e^+ accelerated to E_+= 10 keV.

Fig. 3b shows the time of annihilation for the same geometry but for e^+ accelerated to E_+= 10 keV. Due the higher energy, the delay of the backscattered positrons is smaller which may not only affect the longest-lived component but also the shorter-lived ones in the PALS spectrum. In Fig. 3b an additional, intermediate peak is present right after the initial beam of particles is implanted into the sample. This is due to the fact that for high energies the positrons which are backscattered at a larger angle from the sample will have larger Larmor radii and may hit the wall of the Faraday cage close to the target position (see Fig. 4) and part of them can return to the target after backscattering from the wall (due to the low statistics in the visualization this can't be followed in Fig. 4). The latter effect has been observed previously [14]. One solution is to use a sample chamber with a large diameter. This would however lead to reduced count rates in experiments with detectors placed from the lateral sides. Another solution is to increase the strength of the guiding magnetic field to reduce the Larmor radii [15].

The stop signal in the PALS measurement comes from the detection of the annihilation 511-keV gamma rays. A gamma detector made of BaF_2 was implemented in Geant4 placed right behind the silicon target (see Fig. 2). In order to take into account only events which can produce signal like in a real experiment the gamma quanta that deposited less than 300 keV in the BaF_2 were rejected. Lead

around the gamma detector was used to shield from the gamma rays not originating from the silicon target.

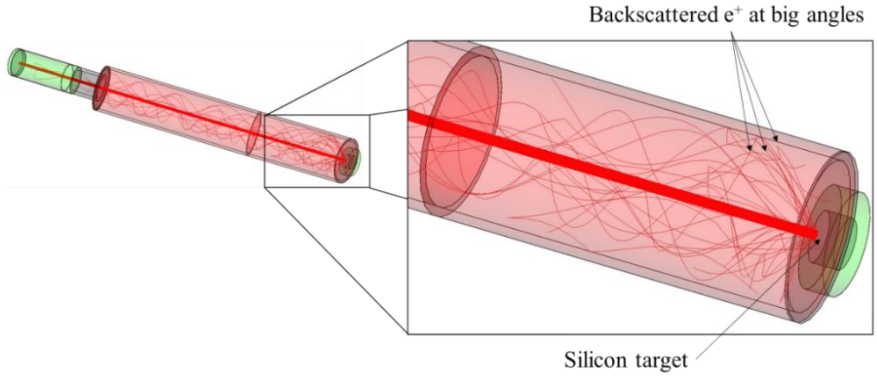

Fig. 4 The trajectories of the primary E_+= 10 keV e^+ beam and the event of e^+ backscattering with 300 incident particles. Example of a straight tube obtained by Geant4. The zoom shows e^+ that are backscattered at a big angle from the sample and hit the walls of the tube close to the target.

The histogram of the time of the gamma rays interaction with the BaF_2 detector obtained by Geant4 in the case of a straight tube and E_+= 2 keV is presented in Fig. 5. The physics models in Geant4 do not account for the e^+ lifetime in a material, therefore the time histogram actually does not represent a PALS spectrum but only the resolution function, $R(t)$. If positrons annihilate from a discrete number of states, the PALS spectrum can be described as a convolution of the resolution function and the probabilities to decay from those states

$$y(t) = R(t) \otimes (N_t \sum_{i=1}^{n} (I_i/\tau_i) exp(-t/\tau_i) + B) \quad ,$$

where τ_i is the lifetime of the i-th state(component), I_i is the intensity of the i-th component, N_t is the total counts and B is the background.

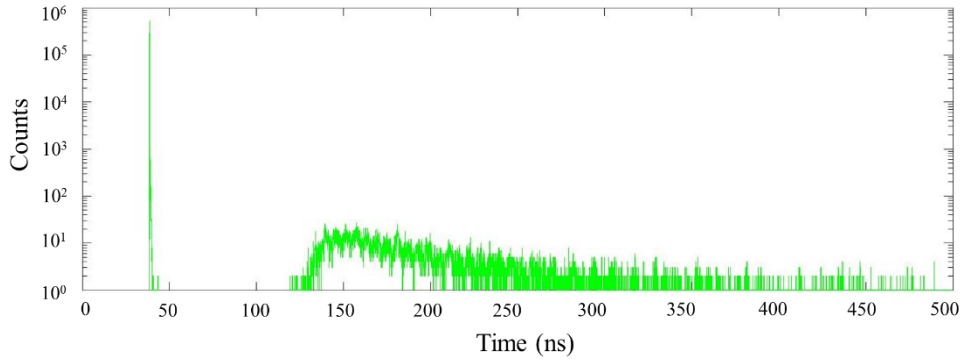

Fig. 5 Histogram of the time of the gamma rays interaction with the BaF_2 detector obtained by Geant4. Example of a straight tube (see Fig. 2) and E_+= 2 keV.

In order to study the effect of backscattered e^+, we simulated PALS spectra convoluting the resolution function $R(t)$ (see Fig. 5) with four components with lifetimes $[\tau_1, \tau_2, \tau_3, \tau_4] = [0.1, 0.5, 3, 20]$ ns and corresponding intensities $[I_1, I_2, I_3, I_4] = [10, 60, 10, 20]$%. The obtained spectrum was also convoluted by a Gaussian with FWHM = 0.15 ns to take into account the typical resolution of a fast gamma detector (BaF_2 coupled with a photomultiplier tube) and Poison noise was added. Example of a simulated spectrum is shown in Fig. 6a. In Fig. 6b a simulated spectrum with suppressed backscattering is shown for a comparison. The distortion in the PALS spectrum introduced by the backscattered e^+ is clearly seen in the example shown in Fig. 6a. In order to quantify the distortion from the model spectrum, the spectra are analyzed by LT9 software [16] to find the best fit parameters and the deviations $\Delta_i = 100 \times \left|\left(P_i - P_i^{fit}\right)/P_i\right|$ ($P = \tau$ or I, and i = 1 to 4) are calculated.

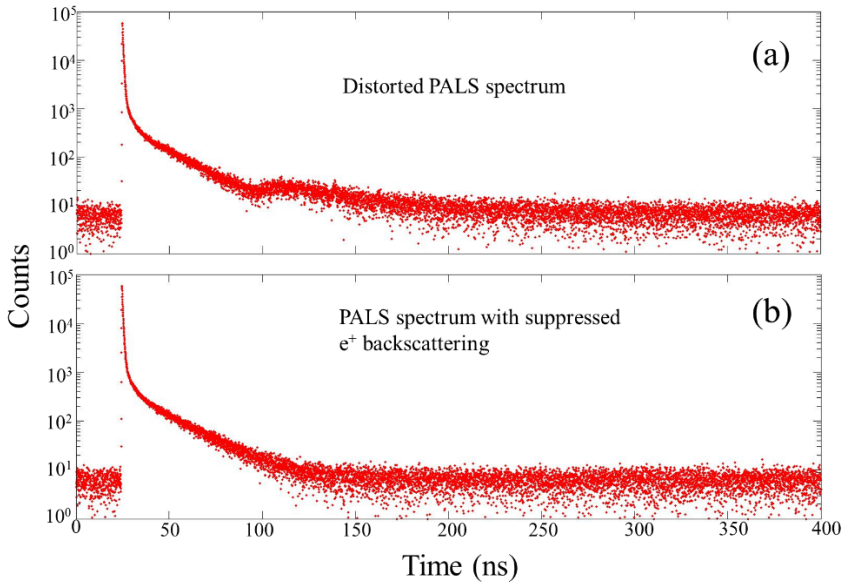

Fig. 6 a) Simulated PALS spectra for a beam of E_+= 2 keV in a straight tube geometry. b) Simulated PALS spectra for a beam of E_+= 2 keV in a straight tube geometry with suppressed e^+ backscattering.

3. Results and discussion

The idea to reduce the effect of the backscattered e^+ on the PALS spectra by using a velocity filter between the accelerator and the sample is motivated by the fact that e^+ are backscattered with longitudinal energy smaller than that one of the incident e^+. Fig. 7 shows the longitudinal energy distribution of e^+, accelerated by U_{acc}= 2 kV, incident on the sample and of the e^+ backscattered from sample.

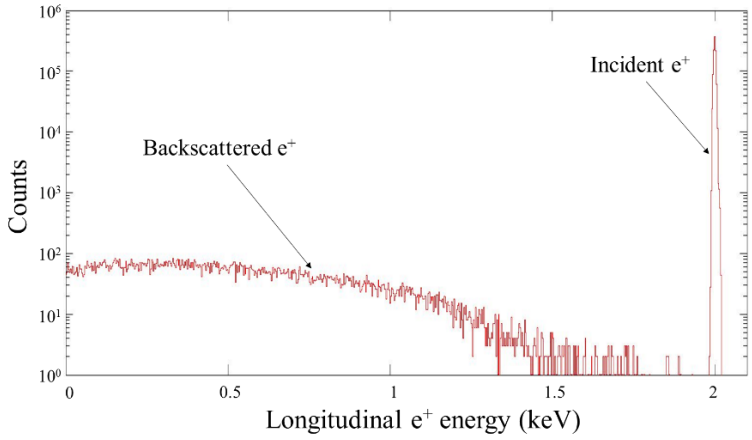

Fig. 7 Longitudinal energy of the incident e^+ (accelerated by U_{acc}= 2 kV) on the sample and of the backscattered e^+ from the sample.

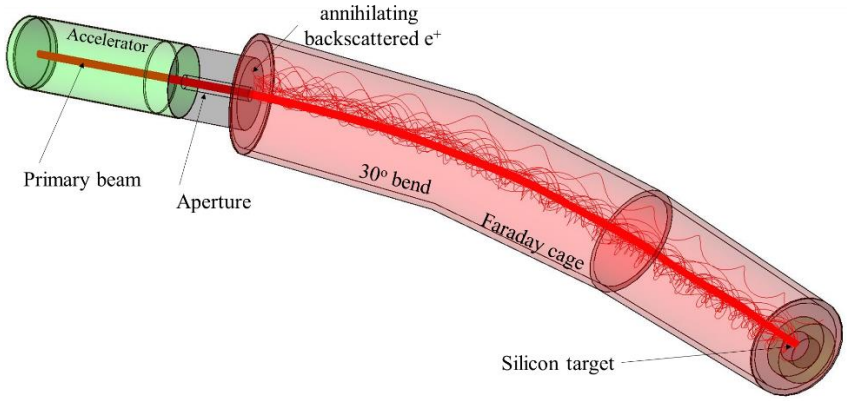

Fig. 8. The trajectories of a 2 keV e^+ beam and the event of e^+ backscattering with 1000 incident particles. Example of a 30˚ bend with an aperture of D = 15 mm obtained by Geant4.

For minimizing the effect of e^+ backscattering, two possible solutions were simulated. The first solution is to add an aperture at the accelerator exit with a diameter, D, comparable with the beam spot size. By applying this measure the primary e^+ beam will pass through the smaller opening towards the sample, but a fraction of the backscattered e^+ will not be able to enter the accelerator through the small aperture and instead they will annihilate on its walls. The second solution is to pass the accelerated e^+ beam through a bent tube equipped with steering coils to act as a velocity filter as shown in Fig. 8. The Faraday cage is composed of two parts: a bent tube with a fixed length of 450 mm followed by a straight part of 270 mm in length. The magnetic field axis generated by the properly placed Helmholtz coils follows the bend and the magnetic field generated by the steering coils is tuned

in such a way that the primary e^+ travel to the target following the central axis of the system. The backscattered e^+ deviate from the axis due to their lower longitudinal energy and will annihilate on the Faraday cage walls far away from the gamma detector.

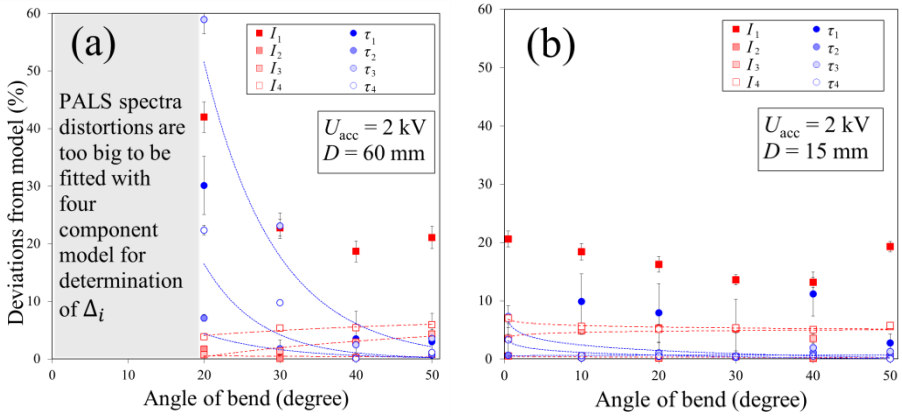

Fig. 9 Fit parameter deviations from the model PALS spectra for a 2 keV e^+ beam without an aperture (a) and with an aperture of D = 15 mm (b) as a function of the bend angle. The trend lines are added (except for τ_1 and I_1) just to guide the eye.

The study was performed for the acceleration potentials U_{acc} = 2, 5, 10 and 20 kV with angles of the bend between 0 and 40˚ following the procedure described in the previous section in order to determine the deviations Δ_i in each case. In Fig. 10 are presented the fit parameter deviations from the model PALS spectra for a 2 keV e^+ beam without an aperture (Fig. 10a) and with an aperture of D = 15 mm (Fig. 10b) as a function of the bend angle. The trend lines are added just to guide the eye. There are no trend lines added for τ_1 and I_1, as they represent the lifetime and intensity of the shortest lived component, which is affected not by the reaccelerated backscattered e^+ but by the e^+ backscattered at big angles annihilating at short distance from the target on the walls of the Faraday cage (see the discussion about Fig. 3b). In addition, it was found that LT9 systematically overestimates the I_1, due to the low ability to resolve correctly the shortest component with the chosen parameters of the instrument resolution. Therefore, their deviations are expected to be independent of the bend angle which is better seen in Fig. 10. Also, it was impossible to do a reasonable fit of the simulated spectra with a four component model in the case without aperture as shown by the shadowed area in Fig. 10a. As the angle of the bend increases, the deviations of the fitted parameters decrease from up to 60% for a 20˚ bend to deviations of less than 10% for a 40˚ bend of the tube (Fig. 10a). If the size of the aperture is reduced to D = 15 mm, comparable to the e^+ beam diameter, the results show that the deviations from the model parameters decrease to below 10% in the case of a straight tube geometry, and, as

the angle of the bend is increased, these deviations start to get closer to the PALS spectrum model parameters ($\Delta_i < 5\%$), as seen in Fig. 10b.

The study was performed for different incident e^+ energies due to the fact that the e^+ backscattering coefficient depends on E_+ [13]. The deviations from the model parameters are decreasing as the bend angle is increased, for E_+ in the interval 2 - 20 keV, showing the same trend lines in all the cases that were studied (Fig. 10). It can be seen that there is a saturation of the deviations at angles $\geq 30^\circ$, meaning that any angle above this value constitutes a viable solution for minimizing the effect of backscattered e^+ by the studied energy filter.

As the energy of the incident e^+ beam increases, the delay of the backscattered e^+ is smaller which means that they will start affecting the shorter lived components as well, as it was discussed in the previous section, and shown in Fig. 3b.

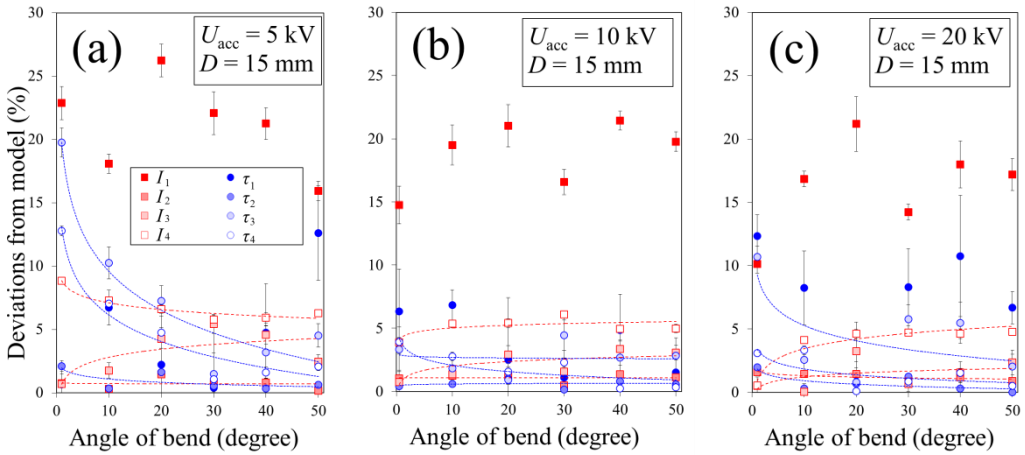

Fig. 10 Fit parameter deviations from the model PALS spectra for a e^+ beam of different energies: a) E_+= 5 keV, b) E_+= 10 keV and c) E_+= 20 keV as a function of the bend angle. The trend lines are added (except for τ_1 and I_1) just to guide the eye.

4. Conclusions

The performed Geant4 simulations have helped to identify the origin of the distortions in the PALS spectra caused by e^+ backscattering. The simulations have shown that adding an aperture at the accelerator exit in combination with bending a part of the Faraday cage, which acts as a velocity filter, is a satisfactory solution to reduce the distortions. The aperture plays an important role and it should be slightly bigger than the maximum diameter of the e^+ beam cross section. The obtained results show that for bend angles $\geq 30^\circ$ the deviation from the model parameters induced by the e^+ backscattering starts to saturate, reaching $\Delta_i < 5\%$ for

E_+ in the interval 2 - 20 keV. The 30^o bend can be considered as an optimal solution which should be sufficient to minimize the effect of the backscattered e^+.

Acknowledgments

The work was supported by the ELI-NP Phase II, a project co-financed by the Romanian Government and the European Union through the European Regional Development Fund - the Competitiveness Operational Program (1/07.07.2016, COP, ID 1334).

R E F E R E N C E S

[1] *P.J. Schultz and K.G. Lynn*, "Interaction of Positron Beams with Surfaces, Thin Films, and Interfaces", in Rev. Mod. Phys., **vol. 60**, 1988, pp. 701-779

[2] *N. Djourelov, C. Hugenschmidt, S. Balascuta, V. Leca, A. Oprisa, C. Piochacz, C. Teodorescu and C.A. Ur*, "Positron Production by Gamma Beam at Eli–Np", in Rom. Rep. Phys., **vol. 68**, 2016, pp. S735-S797

[3] *R.W. Siegel*, "Positron Annihilation Spectroscopy", in Ann. Rev. Mater. Sci., **vol. 10**, 1980, pp. 393-425

[4] *K.G. Lynn, W.E. Frieze and P.J. Schultz*, "Measurement of the Positron Surface-State Lifetime for Al", in Phys. Rev. Lett., **vol. 52**, 1984, pp. 1137-1140

[5] *S.J. Gilbert, C. Kurz, R.G. Greaves and C.M. Surko*, "Creation of a Monoenergetic Pulsed Positron Beam", in Appl. Phys. Lett., **vol. 70**, 1997, pp. 1944-1946

[6] *D. Schödlbauer, P. Sperr, G. Kögel and W. Triftshäuser*, "A Pulsing System for Low Energy Positrons", in Nucl. Instrum. Meth. B, **vol. 34**, 1988, pp. 258-268

[7] *M. Jungmann, J. Haeberle, R. Krause-Rehberg, W. Anwand, M. Butterling, A. Wagner, J.M. Johnson and T.E. Cowan*, "First Experiments with Meps", in J. Phys.: Conf. Ser., **vol. 443**, 2013, pp. 012088

[8] *H. Marinov, N. Djourelov, P. Nédélec and L. Petrov*, "Design, Simulation and Performance of a Slow Positron Beam with Secondary Electron Tagging for Positron Annihilation Lifetime Spectroscopy", in Nucl. Instr. Meth. A, **vol. 729**, 2013, pp. 569-575

[9] *P. Willutzki, J. Stormer, G. Kogel, P. Sperr, D.T. Britton, R. Steindl and W. Triftshauser*, "An Improved Pulsed Low-Energy Positron System", in Meas. Sci. Technol., **vol. 5**, 1994, pp. 548

[10] *W. Egger, P. Sperr, G. Kögel and G. Dollinger*, "Pulsed Low Energy Positron System (Pleps) at the Munich Research Reactor Frm Ii", in Phys. Status Solidi C, **vol. 4**, 2007, pp. 3969-3972

[11] *A. Pelli, A. Laakso, K. Rytsölä and K. Saarinen*, "The Design of the Main Accelerator for a Pulsed Positron Beam", in Appl. Surf. Sci., **vol. 252**, 2006, pp. 3143-3147

[12] Comsol Multiphysics®, Comsol 4.3, Comsol Ab, Stockholm, Sweden, 2012

[13] *J. Makinen, S. Palko, J. Martikainen and P. Hautojarvi*, "Positron Backscattering Probabilities from Solid Surfaces at 2-30 Kev", in J. Phys.: Condens. Matter, **vol. 4**, 1992, pp. L503

[14] *L. Ravelli, B. Löwe, W. Egger, G. Kögel, P. Sperr and G. Dollinger*, "Geant4 Simulation of the Effect of Backscattered Positrons on the Lifetime Spectra of Pleps", in J. Phys.: Conf. Ser., **vol. 443**, 2013, pp. 012096

[15] *K. Fallström and T. Laine*, "Construction of the Helsinki University of Technology (Hut) Pulsed Positron Beam", in Appl. Surf. Sci., **vol. 149**, 1999, pp. 44-48

[16] *J. Kansy*, "Microcomputer Program for Analysis of Positron Annihilation Lifetime Spectra", in Nucl. Instr. Meth. A, **vol. 374**, 1996, pp. 235-244